Effects of Explosion Depth and Crustal Heterogeneity on *Lg* Waves

H. Keers, K. Vogfjörd, G. Nolet, F. A. Dahlen

Department of Geological and Geophysical Sciences, Princeton University, Princeton, NJ 08544

Contract number: F49620-94-1-0077

ABSTRACT

We use ray theory to model the propagation of *Lg* waves through 2D and 3D layered crustal models. The layers are homogeneous, and the discontinuities are undulating. The *Lg* wave train is modelled by multiple *S* reflections within the crustal layers. The ray tracing system is reduced from a set of linear differential equations to a set of maps. If the medium has three or more discontinuities the number of multiples increases exponentially. Using a binary tree-searching method we systematically keep track of all multiples.

The ray behavior is chaotic for large take-off angles, causing multipathing of the crustal multiples. However, in the presence of mid-crustal discontinuities the rms *Lg* amplitude is stable, because of the distribution of the energy over a large amount of rays. The simplest case, a one layer over a halfspace model, already contains all the characteristics of wave propagation through the media under consideration.

To examine the source-depth and velocity-structure effects on amplitudes and character of *Lg* we use wavenumber integration methods in 1-D structures. In particular, we study the ability of shallow explosions to generate S^* and *pS* rays. Although S^* is a nongeometrical phase it does follow a well defined raypath. In velocity structures, where the peak in the S^* radiation pattern is confined to the crust, signals from explosions within 1 km of the surface, that do not generate spall or significant tectonic release, are likely to be dominated by waves with a very narrow ray-parameter range, coming from the radiation peak of S^*. Observation of *Lg* waves dominated by such a narrow ray-parameter range may therefore identify the source as explosive, and shallow. Dislocation radiation patterns, or the spalls CLVD term are likely to generate significant *S* waves over a wider range of ray parameters and therefore not to be confused with S^*.

Effects of Explosion Depth and Crustal Heterogeneity on *Lg* Waves

OBJECTIVE

The objective of our research is to understand aspects of the excitation of *Lg* waves and their subsequent propagation through the crust, including 2D and 3D heterogeneous crustal models.

Modeling the *Lg* wave train is a difficult task, even though measurements of rms amplitude of *Lg* is stable. We attempt to explain this by modeling *Lg* as a superposition of supercritically reflected crustal multiples. In our models the crust is multilayered (2D or 3D) and the interfaces are undulating.

We also examine the effect S^* has on amplitudes and character of *Lg* to determine to what depths and in which types of velocity structures S^* is a significant contributor to *Lg*.

RESEARCH ACCOMPLISHED

Lg Wave Propagation Through 3D Heterogeneous Structures

To study the propagation of *Lg* waves through 2D and 3D heterogeneous media we use ray theory. Ray theory is not only very efficient, it also makes the characterization of *Lg* waves in terms of focusing/defocusing effects, multipathing and traveltimes due to the complicated structure relatively simple. Thus ray theory complements full waveform methods such as finite differences.

Lg waves possess a dual character (e.g. Hansen et al., 1990). On one hand the modeling of *Lg* waves has proved to be very difficult, on the other hand the *Lg* wavetrain has been useful to determine seismic moments because rms *Lg* is a stable quantity, that is relatively independent of regional structure. Using our modeling results we give an explanation for this seemingly contradictory character.

The models that we use are 2D and 3D layered crustal models. The layers are homogeneous, and the discontinuities are undulating. The *Lg* wave train is modelled by multiple *S* reflections within the crustal layers. In a flat layered medium the ray-theoretical seismograms are almost identical to the exact synthetics (Keers et al., 1995a). This serves as our justification for the use of ray theory in media with (slightly) undulating interfaces separated by homogeneous layers.

One of the main advantages of using homogeneous layers is that the ray tracing system can be reduced from a set of linear differential equations to a set of maps (Keers et al., 1994). This makes the ray tracing very efficient; it is not necessary to use a Runge-Kutta method and the search for the point where the ray intersects one of the undulating interfaces is reduced to a 1D root-solving problem (even in the three dimensional case). If the medium has three or more discontinuities the number of multiples increases exponentially. Using a binary tree-searching method we systematically keep track of all multiples.

The simplest case, a one layer over a halfspace model, already contains all the characteristics of wave propagation through the media under consideration. In general two regions (by regions we mean take-off angle intervals) are distinguished. One region, corresponding to smaller take-off angles, has regular ray-behavior, and another region, corresponding to the largest take-off angles, has chaotic ray-behavior. In the case of a sinusoidal Moho with a wavelength of 100 km and an amplitude of 1 km the take-off angle intervals are roughly 50°-65° and 65°-90° (the critical angle is close to 50°). The first region is characterized by a low degree of multipathing and a high degree of focusing. The second region is characterized by a large degree of multipathing and consequently a large degree of defocusing The defocusing is caused by the fact that a small change in take-off angle causes a large change in epicentral distance, except at the caustics. However, at the caustics the amplitude is still relatively small (Keers et al, 1995a). It should be noted that the amplitude perturbations due to the undulation are much larger than the traveltime perturbations. Table 1 gives an

indication of the degree of multipathing for the case of a flat Moho, a sinusoidal Moho and a more realistic model, that of the Moho below Germany.

In the case of a more realistic two-layered model with undulating interfaces, the ray behavior remains essentially the same: there exists a regular region corresponding to smaller take-off angles and a chaotic region corresponding to larger take-off angles. All discontinuities are sinusoidal. The surface has a wavelength of 60 km and amplitude of 0.5 km, the midcrustal discontinuity has a wavelength of 160 km and an amplitude of 0.8 km and the Moho has a wavelength of 100 km and an amplitude of 1.5 km. Figure 1a shows the amplitude distribution. This figure is essentially an 'envelope record-section'. It contains only amplitude information; no phase information. The strong focusing in the regular region that was present in the one-layered model is gone. This is due to the reflection and transmission of the multiples at the midcrustal interfaces, which partitions the energy over many multiples. The presence of the chaotic region makes it impossible to identify even the major multiples (SmS, $2SmS$ etc.) at larger epicentral distances. The large degree of multipathing of a certain multiple, like $2SmS$, causes these multiples to consist of many rays, each with a relatively small amplitude, coming in from totally different directions. Each of these multiples is smeared out over a larger time interval and the the maximum amplitude of the dominant rays is low compared to the flat layered case. This explains why the modeling of Lg waveforms has been largely unsuccesful: the waveform is very sensitive to initial conditions (take-off angle) and model parameters.

Figure 2a shows the effect of a 3D sinusoidal Moho. The wavelength is 100 km in both the x and y directions, and the amplitude is 1 km. The figure shows the energy distribution along the x axis. Also shown is the energy distribution for a 2D model with a sinusoidal Moho that has a wavelength of 100 km and amplitude of 1 km. The amount of side scattering can not be ignored, but depends strongly on the model (Keers et al, 1995b). Since this 3D example is for a one-layered model, the focusing of the different multiples plays a dominant role in this figure.

Figure 2b shows the total energy of the Lg wavetrain as a function of epicentral distance for the two models of figure 1. Also plotted is the energy of the waves assuming a $\Delta^{-5/6}$ (Nuttli, 1973) decay of the amplitude (Δ=distance). The undulating two-layered model shows much less focusing especially at larger epicentral distances. This is due to the midcrustal interface. There is still focusing of certain rays, but the reflection and transmission from the midcrustal interface makes these rays much less dominant than in the one-layered model. This explains the stability of rms Lg as observed for many regional events (e.g. Hansen et al., 1990). For models with more layers we can expect the focusing effects to become even less dominant.

Effects of Source Depth and Velocity Structure on the Character of Lg

Discrimination between shallow sources is a difficult task and methods, such as Pg/Lg amplitude ratios and Lg spectral ratios as well as regional m_b:M_S, seem to be region dependent and only work for discrimination between shallow explosions and earthquakes deeper than 5 km, and even then there are problems with explosion depths of <1 km. Generation of S waves from explosion sources has generally been attributed to nonisotropic source radiation, spall, tectonic release, or Rg-S scattering in the source region, while S^*, the wave generated by interaction between the curved P wave-front and the surface, has usually been discounted for all but the shallowest sourcs, because of its strong dependence on source depth. However, due to the S^* radiation pattern, in certain structures the amplitude may be significant down to depths of ~1 km, possibly making S^* an added tool to discriminate between shallow sources.

To examine the source-depth and velocity-structure effects on amplitudes and character of Lg we use wavenumber integration methods in 1-D structures. The shortcomings of the simplified structure are overcome by the benefits of a full-wave synthesis, revealing all waves generated by the source and its interaction with discontinuities in the structure; of main interest, of course, is the interaction with the Earth's surface. The characteristics observed in the synthetics are then explained in terms of the radiation pattern of S^*.

A high frequency approximation to the amplitude and phase of the S^* wave was developed by Daley and Hron (1983). In this approximation S^* appears as a spherical wave-front with SV-particle motion, radiated from a point on the surface above the source. Its amplitude is modulated as a function of angle ϕ (measured from the vertical), but is independent of azimuth. The wave exists for $\phi_d = \sin^{-1}(\beta/\alpha) \leq \phi \leq \pi/2$, but the approximation is valid for $\phi_d < \phi < \pi/2$, or $1/\alpha < p < 1/\beta$, where α and β are the mediums P and S

velocities and $p = \sin\phi/\beta$, is the ray parameter. A plot of the radiation function for a frequency of 2 Hz and $\alpha = 4.2$ km/s is shown in Figure 3 (top right). The source depths represented are: 0.1, 0.5, 1.0 and 2.0 km. The amplitude is a maximum at ϕ_d, but decreases to zero at $\phi = 45°$, where the phase also flips by 90°. The amplitude increases again to a smaller maximum, before becoming zero again at 90°. The amplitude decays exponentially with source depht, so for depths greater than 0.5 km, amplitudes are very small at angles above 45°. However, between ϕ_d and 45° the amplitude can be larger than in the original P and the reflected pS wave. To demonstrate, the pS radiation pattern, which exists for reflection angles $\phi < \phi_d$, is also included on the plot.

If the narrow radiation peak of S^* gets trapped in the crust, it may dominate Lg. To demonstrate we calculated synthetics in three different velocity structures, md1, where the peak is radiated into the mantle, md2, where the peak is confined to SmS multiples for source depths down to 1.25 km and, md3, where the peak is confined to turning waves in the crust for source depths down to 1 km. The models have a common Q structure and share a velocity structure below 3 km depth (see Figure 4, lower panel). It is the ratio $\alpha_{source}/\beta_{mantle}$ that determines how much of S^* is trapped in the crust. If $\alpha_{source} < \beta_{mantle}$, all of S^* and some pS are contained in Lg, but when α_{source} increases to $\geq \beta_{mantle}$ the radiation peak starts to go into the mantle. When the critical angle for Moho reflection exceedes $\sim 42°$, no significant S^* can be found in Lg, except for depths $\leq$0.5 km. The angular range of Moho reflections in the three models is indicated on Figure 3 (top right). There it is clear that in md1, most of the S^* radiation peak goes into the mantle and therefore Lg, from a pure explosion source, is expected to decay quickly with source depth. However in md2, all of the radiation peak ends up in Moho reflections, for source depths down to 1.25 km. For this depth range Lg is expected to be of significant amplitude and to be dominated by Moho reflections. In md3, the peak is confined to turning waves in the crust, for source depths down to 1 km. In this depth range Lg is also expected to be significant and dominated by turning waves. These effects are clearly seen in the synthetics: In Figure 4, synthetics are shown at a distance of 500 km for source-depths ranging from 0.1 to 2 km in model md2. Clearly the Lg wave is dominated by the Moho multiples, $2SmS$, $3SmS$ and $4SmS$, and Lg amplitude is significant for source depths down to $\sim$1 km. Record sections for an explosion source at 0.5 km depth in the three models are shown in Figure 5, where the expected features are also seen. The md1 record section has smaller amplitude Lg waves than the other models, evenly divided between Moho reflections and turning waves. The frequency content of the Lg wave is also significantly lower than that of the crustal P wave-train. The md2 record section has much larger amplitudes, Lg is dominated by Moho multiples, and there is no significant loss of higher frequencies in Lg. The md3 record section has large amplitude Lg waves of high frequency content, and maximum amplitudes coincide with the arrivals of the turning waves and Moho reflections; the Moho reflections come from pS and the turning waves come from S^*.

Analysis of Array Data

The theoretical results need to be tested against observed data from local and regional events. We have so far selected two regions based on the availability of short-period array data. The regions are: Central Europe, where we make use of the GERESS array, and the Sierra Nevada, where three, 3-component arrays were temporarily operated in 1993. The arrays enable detection of small coherent arrivals and decomposition of the Lg wave train into distinct arrivals with differing phase velocities. The events recorded at GERESS consist of earthquakes and explosions, while most of the events recorded on the Sierra Nevada arrays are earthquakes, but also include the NPE explosion at the Nevada Test Site in September 1993.

CONCLUSIONS AND RECOMMENDATIONS

In 2D and 3D heterogeneous media Lg wave propagation is strongly affected by curved interfaces. The ray behavior is chaotic for large take-off angles, causing multipathing of the crustal multiples. This makes modeling of Lg waves a tidy task. However, in the presence of mid-crustal discontinuities rms Lg is stable, because of the distribution of the energy over a large amount of rays. It should be noted that the undulations used are small (of the order of 1 km). The amplitude behavior will change if the undulations of the Moho become large. Further research is needed to establish this effect. Incorporation of P-S and S-P conversions using our ray-tracing algorithm should make it possible to model Lg wave propagation more realistically.

More detailed Moho maps for regions of interest are also necessary for reliable modeling of *Lg* in 3D structures. This goal can be achieved by wave-form inversion, using regional seismograms (Das and Nolet, 1995).

In velocity structures, where the peak in the S^* radiation pattern is confined to the crust, signals from explosions within 1 km of the surface, that do not generate spall or significant tectonic release, are likely to be dominated by waves with a very narrow ray-parameter range, coming from the radiation peak of S^*. Observation of *Lg* waves dominated by such a narrow ray-parameter range may therefore identify the source as explosive, and shallow. Dislocation radiation patterns, or the spalls CLVD term are likely to generate significant S waves over a wider range of ray parameters and therefore not to be confused with S^*. A comparison between data from mining explosions and earthquakes, located in approximately the same area, may serve as a test case for this. GERESS data for events in the Vogtland region in the Czech Republic may be possible candidates.

The completed record section profiles will serve as the data base needed to test the validity of the theoretical calculations and predictions.

REFERENCES

Daley, P. F. and F. Hron (1983). High-frequency approximation to the nongeometrical S^* arrival, *Bull. Seism. Soc. Am.*, **73**, 109-123.

Das, T. and G. Nolet (1995). Crustal thickness estimation using high frequency Rayleigh waves, *Geophys. Res. Lett.*, **22**, No. 5, 539-542.

Hansen, R. A., F. Ringdal and P. G. Richards (1990). The Stability of RMS *Lg* Measurements and Their Potential for Accurate Estimation of the Yields of Soviet Underground Nuclear Explosions, *Bull. Seism. Soc. Am.*, **80**, 2106-2126.

Keers, H., G. Nolet and F. A. Dahlen, 1995a. Ray Theoretical Analysis of *Lg*, (submitted to *Bull. Seism. Soc. Am.*).

Keers, H., G. Nolet and F. A. Dahlen, 1995b. Chaos and *Lg* Waves, EOS, volume 76, no 17, 205.

Keers, H., K. Vogfjörd, G. Nolet and R. Phinney, 1994. *Lg* Synthesis in Media With Undulating Surfaces by Ray Summation, EOS, volume 75, no 44, 420.

Nuttli, O. W. (1973). Seismic wave attenuation and magnitude relations for Eastern North America, *J. Geophys. Res.*, **78**, 876-885.

Vogfjörd, K. S. (1995). Effects of explosion depth and Earth structure on excitation of *Lg*: S^* revisited, (submitted to *Bull. Seism. Soc. Am.*).

Table 1 Number of supercritically reflected rays for different Moho models

epicentral distance (km)	flat Moho	Sinusoidal Moho	Moho below Germany
200	4	4	17
300	6	6	26
400	8	10	53
500	10	14	140
600	12	22	216
700	15	31	218
800	17	56	270

Table 2	layer #	thickness (km)	S-velocity (km/s)	density (g/cm3)
	1	15	3.5	2.7
	2	15	3.9	3.1
	3	∞	4.6	3.3

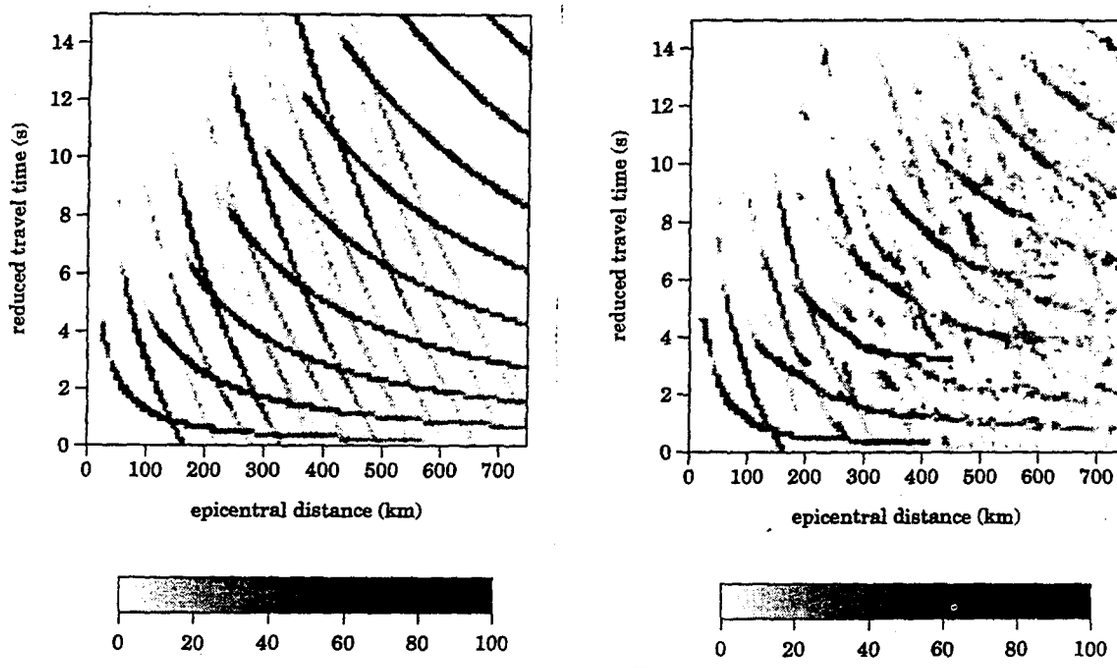

Figure 1. Amplitude distribution for two-layered crustal model with flat interfaces (left) and undulating interfaces (right; see text for the characteristics of the undulations). The amplitudes are scaled with respect to the maximum value (100).

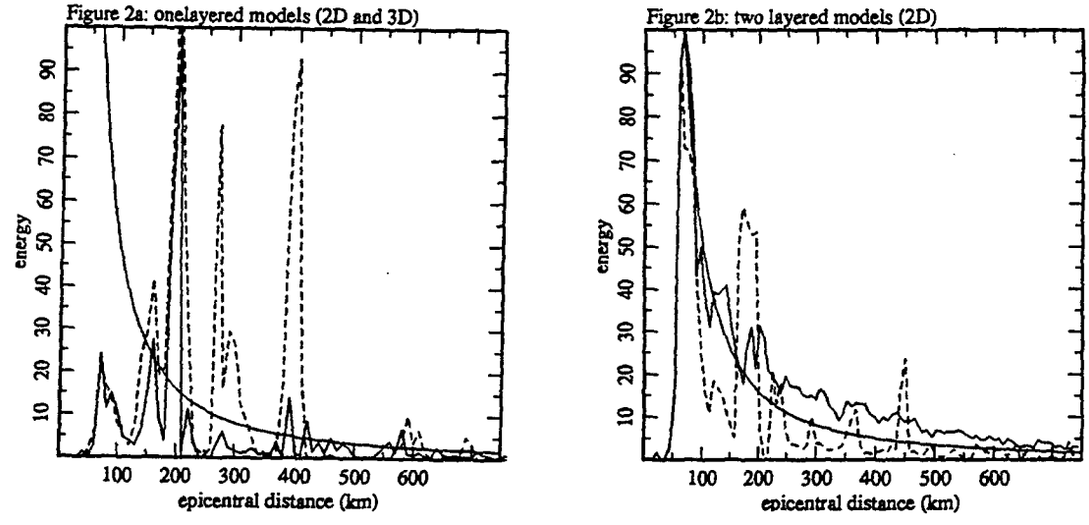

Figure 2a. Energy distribution for a one-layered crustal model with undulating Moho (see text) for 2D (solid) and 3D (dashed) model. The decay of energy according to Nuttli (1973) is also shown (smooth curve).

Figure 2b. Energy distribution for same models as in figure 1: flat model (solid) and model with undulating discontinuities (dashed). The smooth curve is the decay of energy according to Nuttli (1973).

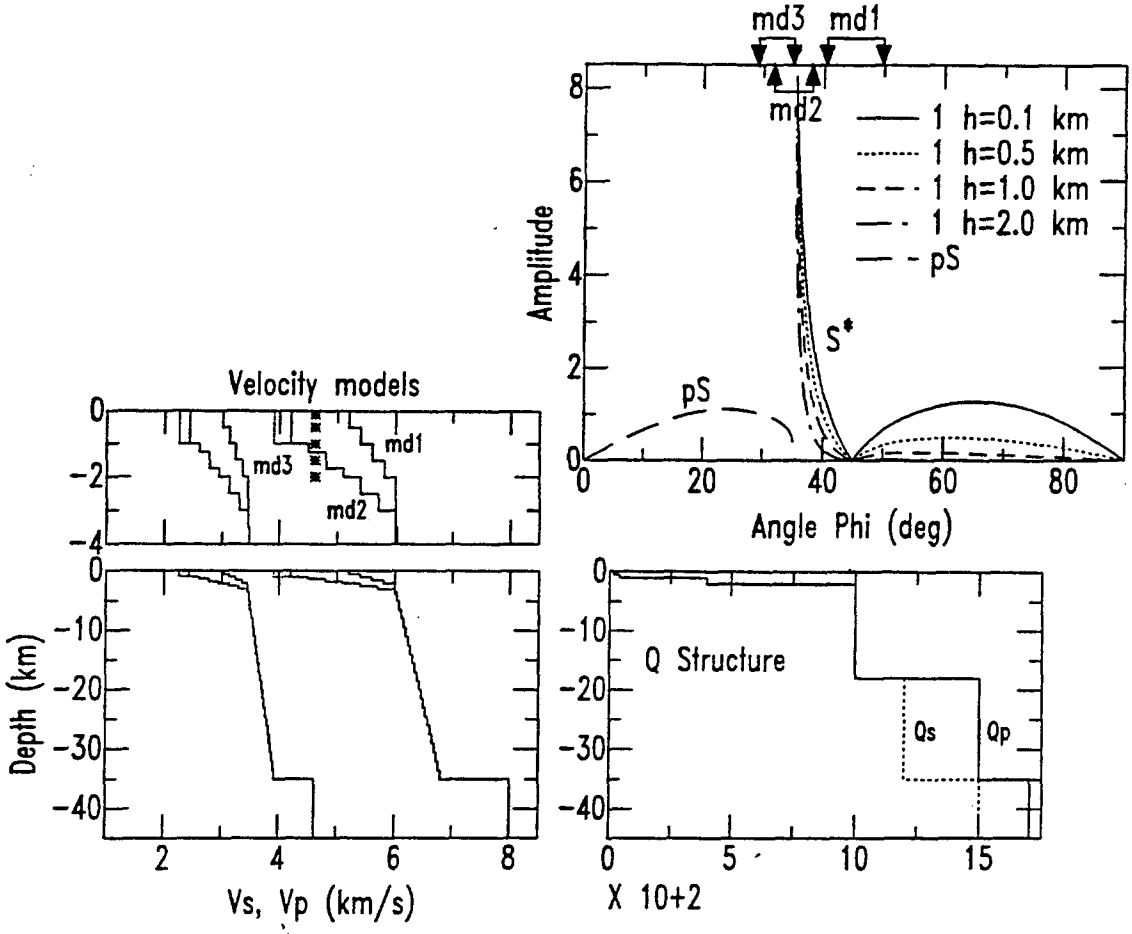

Figure 3. (upper right) S^* radiation pattern at 2 Hz, for various source depths in a medium with $\alpha = 4.2$ km/s. Velocity models (left) and Q structure (lower right) used in the synthetic calculations. Stars, representing some of the source depths used, are positioned at the sub-Moho S velocity, β_{mantle}.

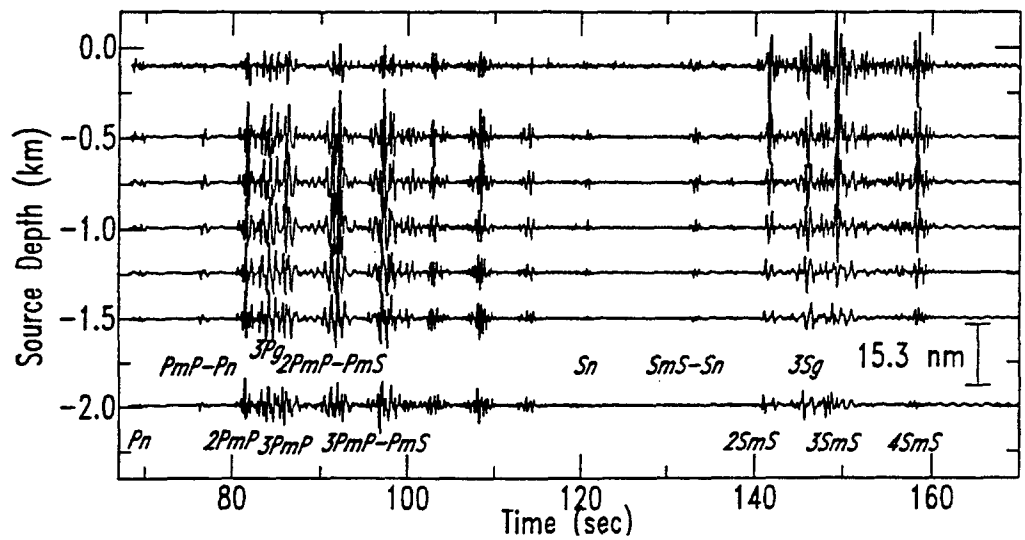

Figure 4. Vertical component synthetic displacement at 500 km distance from an explosion source at various source depths in model md2. The synthetics have a Nyquist frequency of 4 Hz and are convolved with a NORESS-type short-period instrument.

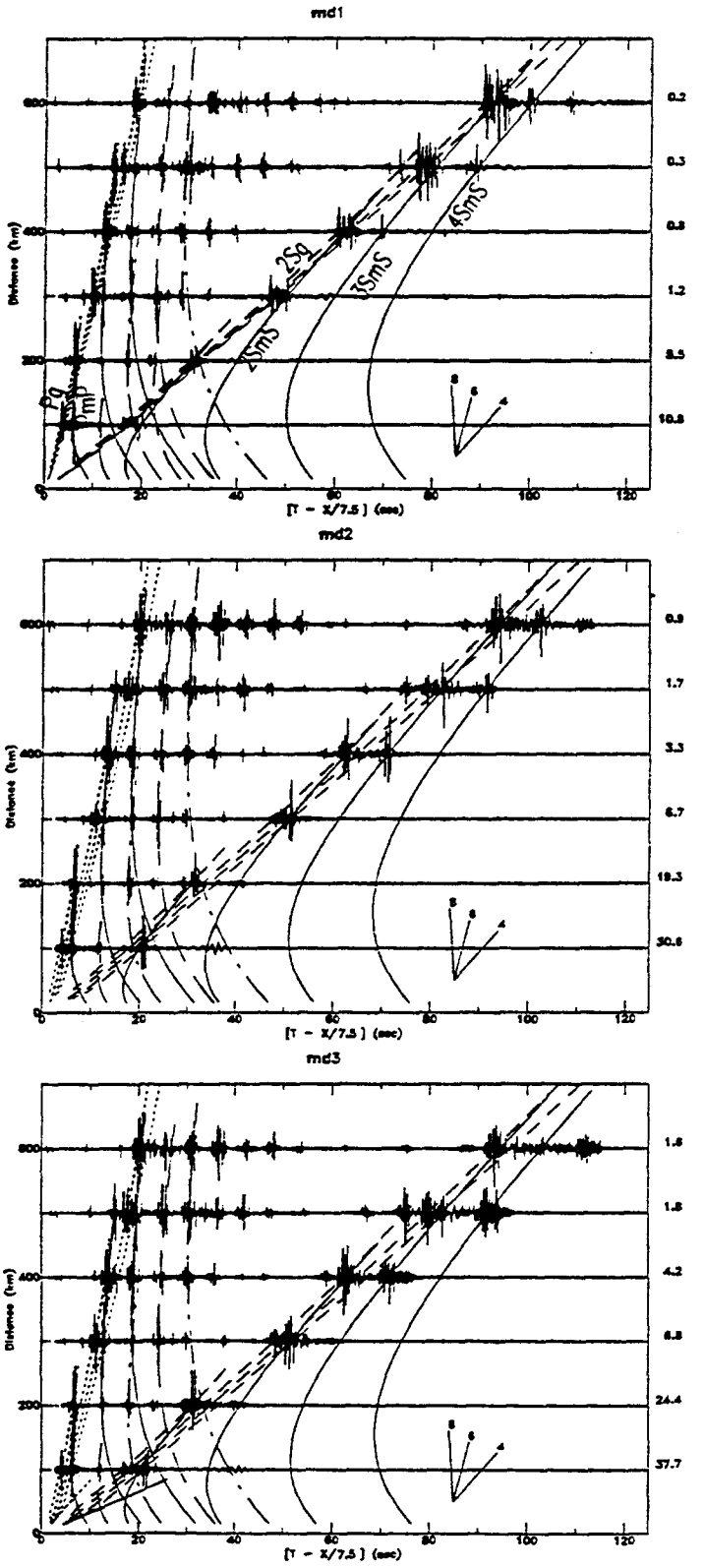

Figure 5. Vertical component synthetic record sections for an explosion depth of 0.5 km in the three models, md1, md2 and md3, with travel-time curves for the major phases superimposed. Amplitudes are normalized to their maxima, shown at the right of each trace. Slopes on the travel-time curves can be read from the velocity template in the lower right corner.